GMe Forum 2005

Abstracts of the Poster Presentations

Vienna University of Technology
March 17 and 18, 2005

Society for Micro- and Nanoelectronics
Vienna, 2005

Society for Micro- and Nanoelectronics
c/o Institute of Sensor and Actuator Systems
Vienna University of Technology
Gusshausstrasse 27–29/366
A-1040 Vienna, Austria

Opto-Electronics:

G. FASCHING et al. (TU Vienna): "*Terahertz Quantum Cascade Lasers Operating in Magnetic Fields*"

T. FROMHERZ et al. (JKU Linz): "*SiGe Quantum Cascade Structures for Resonant Cavity Enhanced Two-Color Mid-Infrared Detection*"

M.V. KOVALENKO et al. (JKU Linz): "*Chemically Synthesized HgTe Nanocrystals for the Telecommunication Wavelength Range*"

C. PFLÜGL et al. (TU Vienna): "*Surface-Emitting Single-Mode Quantum Cascade Lasers*"

Photonic Crystals:

E. BAUMGARTNER et al. (JKU Linz): "*Epitaxial Bragg Mirrors with Broad Omnidirectional Stop Bands in the Mid-Infrared*"

T. GLINSNER et al. (JKU Linz): "*UV-Nanoimprinting – A Potential Method for the Fabrication of 3D-Photonic Crystals*"

V. RINNERBAUER et al. (JKU Linz): "*Polarization Splitting Based on Planar Photonic Crystals*"

Spintronics:

A. BONANNI et al. (JKU Linz): "*Electronic and Magnetic Properties of GaN:Fe*"

D. GRUBER et al. (JKU Linz): "*High Mobility Si/SiGe Heterostructures for Spintronics Applications*"

Quantum Dots:

W. BREZNA et al. (TU Vienna): "*Quantitative Scanning Capacitance Spectroscopy on GaAs and InAs Quantum Dots*"

G. CHEN et al. (JKU Linz): "*Self-Organisation of Ripples and Islands with SiGe-MBE*"

G. FASCHING et al. (TU Vienna): "*Photocurrent Spectroscopy of Single InAs/GaAs Quantum Dots*"

G. PILLWEIN et al. (JKU Linz): "*Lateral Quantum Dots in High Mobility Heterostructures*"

M. SCHRAMBÖCK et al. (TU Vienna): "*Self Organized InAs Quantum Dot Arrays on Patterned GaAs Substrates*"

F.F. SCHREY et al. (TU Vienna): "*Ultrafast Intersublevel Spectroscopy of a Single Quantum Dot*"

J. STANGL et al. (JKU Linz): "*X-Ray Diffraction from a SiGe Island Quasicrystal*"

Ballistic Electron Emission Microscopy:

D. RAKOCZY et al. (TU Vienna): "*Cross Sectional Ballistic Electron Emission Microscopy for Schottky Barrier Height Profiling on Heterostructures*"

Organic Semiconductors:

Th.B. SINGH et al. (JKU Linz): "*High Electron Mobility Organic Field-Effect Transistors using Fullerene Thin Films*"

ESD Protection:

V. DUBEC et al. (TU Vienna): "*Thermal Imaging at Multiple Time Instants for Study of Self-Heating and ESD Phenomena*"

J. KUZMÍK et al. (TU Vienna): "*Degradation Mechanisms in AlGaN/GaN HEMTs under Electrostatic Discharge*"

Electron and Ion Beam Processes:

M. FISCHER et al. (TU Vienna): "*Direct-Write Deposition Utilizing a Focused Electron Beam*"

A. LUGSTEIN et al. (TU Vienna): "*A New Approach for the Formation of Size and Site Controlled Metallic Nano Dots Seeded by Focused Ion Beams*"

Plasma Processing:

S. GOLKA et al. (TU Vienna): "*Inductively Coupled Plasma Reactive Ion Etching of GaN*"

Sensors and Sensor Technology:

B. JAKOBY et al. (TU Vienna): "*Analytical 3D Hydrodynamical Analysis of Spurious Compressional Wave Excitation by Microacoustic TSM Liquid Sensors*"

F. KEPLINGER et al. (TU Vienna): "*Simultaneous Measurement of Two Magnetic Field Components Using a Single U-Shaped MEM Cantilever Device*"

J. KUNTNER et al. (TU Vienna): "*Oil Condition Monitoring Using a Thermal Conductivity Sensor*"

M. MÜNDLEIN et al. (TU Vienna): "*Microsensor for the Measurement of the Transepidermal Water Loss of Human Skin*"

J.H. NIEUWENHUIS et al. (TU Vienna): "*Particle Discrimination with an Improved Projection Cytometer*"

P. Svasek et al. (TU Vienna): "*SU-8-Based Fluidic Devices*"

Terahertz Quantum Cascade Lasers Operating in Magnetic Fields

G. Fasching [1], R. Zobl [1], V. Tamošiunas [1], J. Ulrich [1], G. Strasser [1], K Unterrainer [1], R. Colombelli [2], C. Gmachl [2], L.N. Pfeiffer [2], K.W. West [2], and F. Capasso [3]

[1]Institute of Photonics and Center for Micro- and Nanostructures, Vienna University of Technology, A-1040 Vienna, Austria

[2]Bell Laboratories, Lucent Technologies, 600 Mountain Avenue, Murray Hill, NJ 07974, USA

[3]Harvard University, Division of Engineering and Applied Sciences, Cambridge, MA 02138, USA

Terahertz quantum-cascade lasers (QCLs) are coherent sources of far-infrared radiation based on semiconductor heterostructures. Operation of QCLs in the Terahertz range of the electromagnetic spectrum was demonstrated recently by Köhler *et al*. [1]. Further improvement of the THz QCLs is a challenge for several reasons related to the intersubband population dynamics and to the waveguide properties. Electron-electron and interface roughness scattering represent the main scattering mechanisms at low temperatures in this range of intersubband energies. The additional quantization (induced by the magnetic field) of the in-plane electronic motion dramatically modifies the electron-electron scattering and affects the overall performance of the QCL.

In this contribution, we report on the behavior of THz QCLs in an external magnetic field, applied perpendicular to the epitaxial layers. The experimental setup consists of a cryostat with superconducting magnets (one for the THz emitter and one for the InSb detector), a Nicolet FTIR spectrometer and a 4.2 Si bolometer. Clear emission intensity oscillations were observed when changing the sample magnetic field. The substantial emission intensity improvement may be attributed to an increase of the injector efficiency and to a reduced probability of non-radiative transitions in the active region at certain magnetic field values [2]. In addition, a modulation of waveguide properties has to be taken into account when describing the overall performance of the QCL [3]. Substantial emission line shifts, well exceeding the conventional Stark shift, were observed when increasing the magnetic field from 3.2 T to 6.2 T. Many body effects and a modulation of the Bloch gain can cause such shifts.

[1] R. Köhler, A. Tredicucci, F. Beltram, H. E. Beere, E. H. Linfield, A. G. Davies, A. Ritchie, R. C. Iotti, F. Rossi, Nature **417**, 156 (2002).

[2] V. Tamosiunas, R. Zobl, J. Ulrich, K. Unterrainer, R. Colombelli, C. Gmachl, K. West, L. Pfeiffer, F. Capasso, Appl. Phys. Lett. **83,** 3873 (2003).

[3] V. Tamosiunas, R. Zobl, G. Fasching, J. Ulrich, G. Strasser, K. Unterrainer, R. Colombelli, C. Gmachl, K. West, L. Pfeiffer, F. Capasso, Semicond. Sci. Techn. **19,** 348 (2004).

SiGe Quantum Cascade Structures for Resonant Cavity Enhanced Two-Color Mid-Infrared Detection

T. Fromherz, M. Grydlik, P. Rauter, and G. Bauer
Institute of Semiconductor and Solid State Physics
Johannes Kepler University, A-4040 Linz, Austria

P-type-doped SiGe heterostructures originally designed to operate as injectors for quantum cascade electroluminescence and grown by low-temperature molecular beam epitaxy have been demonstrated to be capable of voltage-tunable two-color mid-infrared photodetection. The onset wavelength of the structure's detectivity can be tuned from 3.6 µm to 10.3 µm by applying voltages from –8 to +9 volts to the mesa contacts. The peak detectivity can be switched from 3.1 µm to 4.9 µm by reversing the sign of the bias voltage. The detectivity spectra are relatively broad, and peak detectivities are one order of magnitude lower than those for III-V-detectors in the same wavelength region.

As the detectivity peaks of the cascade structure are located around 3 and 5 µm, a properly designed cavity would enhance infrared detection of two wavelengths (ratio 2:1) situated in each of the both responsivity regions. Thus voltage-induced switching between two detectivity wavelengths can be made more efficient by narrowing the detectivity peaks and increasing their maximum using a resonator cavity.

The resonator cavity is produced by etching squares into the back side of the sample in order to deposit a mirror (in the simplest case made of gold) beneath the heterostructure mesa. Thermal buried SiO_2 is used as an etch-stop to define a planar surface on which the mirror can be deposited.

SiGe quantum cascade structures have been grown on SOI substrates and have been demonstrated to show the same detectivity behavior as structures grown on Si substrates.

An extensive series of etching experiments has been carried out with various combinations of etchants and mask materials and showed that the best-working process includes masking the sample's back side with subsequent layers of benzocyclobutene and SiN and using tetramethyl ammonium hydroxide as an etchant. The produced cavities show flat surfaces and perfect square shape defined by the Si crystal planes.

In addition to the research into cavity fabrication, band-structure simulations have been performed to further optimize structure design and to introduce new concepts for increasing the structure's detectivity by decreasing its noise current and for shifting detectivity spectra to shorter wavelengths by using Si_xGe_{1-x} pseudo-substrates.

In order to study infrared absorption and tunnelling processes on semi-relaxed structures grown on $Si_{0.8}Ge_{0.2}$ pseudo-substrates, several periods of a combination of single quantum wells and barriers of different heights and widths have been grown and investigated by photocurrent spectroscopy measurements.

Future experiments will include time-resolved measurements on different SiGe heterostructures, in order to gain life-time information on well states for simulation and design purposes.

Chemically Synthesized HgTe Nanocrystals for the Telecommunication Wavelength Range

M.V. Kovalenko, J. Roither, E. Kaufmann, and W. Heiss
Institute of Semiconductor and Solid State Physics
Johannes Kepler University, A-4040 Linz, Austria

The development of modern telecommunication networks requires the creation of efficient emitters at wavelength of 1.3 and 1.55 μm close to the low-loss windows of currently used optical fibers. Highly-efficient photoluminescence (PL) of colloidally prepared semiconductor nanocrystals (NCs) and size tunability make NCs very attractive for applications in light-emitting devices. So far, however, chemical synthesis of high-quality NCs is well-established only for wide bandgap materials emitting in the visible spectral region.

Here, we report on an aqueous-based colloidal synthesis of HgTe NCs with strong near-infrared PL, tunable in the wavelength range between 1.1 and 2.4 μm, using a variety of thiols as stabilizers. In contrast to previous reports on thioglycerol-capped HgTe NCs [1] we show the possibility to keep the PL quantum efficiency high during their growth. This is obtained by thermal annealing of as synthesized NCs emitting at 1.2 μm in aqueous solutions, followed by a ligand exchange procedure, resulting in differently sized HgTe NCs with PL peak-positions up to 2.4 μm. These HgTe NCs are stable over months in either powdered form or being dispersed in a variety of matrixes (solvents, polymers etc.) without considerable changes in their optical properties, even under storing at ambient conditions. By the choice of the capping thiol molecules we demonstrated the possibility to provide different surface functionalities making NCs soluble in a variety of solvents. HgTe NCs capped by thioalcohols or thioacids show hydrophilic surface functionality and are soluble in water as well as mixable and compatible with other polar or charged species (polyelectrolites, surfactants etc.). HgTe NCs capped by aliphatic monothiols are typically hydrophobic with high solubility in organic solvents (such as toluene, chloroform etc.) and compatible with nearly all kinds of organic-soluble polymers. This opens great opportunities for the creation of the new functional materials via incorporation of HgTe NCs into variety of matrixes.

In order to show perspectives for the application of HgTe NCs in optoelectronic devices we have prepared two types of highly luminescent HgTe NCs/polymer composite films. The first concept utilizes layer-by-layer deposition techniques [2] where alternating deposition of monolayers of HgTe NCs and polyelectrolytes is used to obtain films with a well controllable thickness. The second concept makes use of hydrophobic HgTe NCs which are mixed into organic-soluble polymers. The NCs-polymer blend is then spin-cast on various substrates, resulting in homogeneously thin films with uniformly distributed HgTe NCs. The films prepared by both of these concepts can act as active material in optoelectronic devices like lasers or optical amplifiers and solar cells.

[1] A. Rogach *et al.*, Adv. Mater. **11**, 552 (1999).

[2] G. Decher, Science **277**, 1232 (1997).

Surface-Emitting Single-Mode Quantum Cascade Lasers

C. Pflügl, M. Austerer, S. Golka, W. Schrenk, T. Roch, A. M. Andrews, M. Schramböck, and G. Strasser
Center for Micro- and Nanostructures
Vienna University of Technology, A-1040 Vienna, Austria

Significant improvements during the last decade made QCLs [1] interesting for many applications, where coherent light emitters in the mid- and far-infrared are required. An important step for the use of these devices was the achievement of single mode emission. This was first demonstrated by processing the lasers as first order distributed feedback (DFB) lasers, where a grating, which is imposed on top of the laser, selects a single mode within the gain spectrum of the device. [2], [3]

QCLs are based on intersubband transitions. Selection rules for transitions in quantum wells allow gain only for TM polarized electromagnetic waves. Therefore, conventional vertical cavity surface emitting laser design is not suitable for QCLs. If one wants to exploit the advantages of surface-normal emission another approach must be taken. One successful way to achieve surface emission is to use two-dimensional photonic crystals [4] or a distributed feedback design where the feedback is given through a second-order Bragg grating etched into the surface of the laser ridge [5], [6].

We present surface emitting QCLs in the two main material systems GaAs and InP. The GaAs QCLs were grown by solid source epitaxy and the InP QCLs by metal-organic vapor phase epitaxy. The grating was exposed on top of the material by means of optical lithography and reactive ion etching (RIE). The grating peaks were covered with Au metal in order to provide a homogenous current distribution across the laser ridges, which are also defined by RIE.

The emitted power for the GaAs-based devices, via the surface, is in the range of a few Watts (@ 78K) and exceeds the emitted power from the uncoated facets. A double-lobed surface emission farfield pattern is obtained for the lasing mode from the DFB gratings without phase shift. The single mode emission wavelength (~9 μm) is continuously tunable by the heat sink temperature [7]. The InP devices emit at about 7.8 μm and are working well above room temperature. The surface emission power of these devices exceeds 1W at RT. Thus, as well as tunable single-mode surface emission on Peltier coolers, these devices provide very high surface emission power for this temperature range. [8]

[1] J. Faist et al., Science 264, 553 (1994)

[2] J. Faist et al., Appl. Phys. Lett. 70, 2670 (1997)

[3] W. Schrenk et al., Appl. Phys. Lett. 76, 253 (2000)

[4] R. Colombelli et al., Science 302, 1374 (2003)

[5] D. Hofstetter et al., Appl. Phys. Lett. 75, 3769 (1999)

[6] W. Schrenk et al., Appl. Phys. Lett. 77, 2086 (2000)

[7] C. Pflügl et al., Opto.Electron. Rev. 12(4), 361 (2004)

[8] C. Pflügl et al., Appl. Phys. Lett., in print

Epitaxial Bragg Mirrors with Broad Omnidirectional Stop Bands in the Mid-Infrared

E. Baumgartner, T. Schwarzl, G. Springholz, and W. Heiss
Institute of Semiconductor and Solid State Physics
Johannes Kepler University, A-4040 Linz, Austria

Omnidirectional Bragg reflectors offer, similar to metallic mirrors, high reflectivity independent of the angle of incidence, but combined with the low-loss behavior and transparency of dielectric multilayer stacks. Thus, these devices are advantageous for applications in laser resonators where light is incident from oblique directions, as in low-loss ring resonators or in two-dimensional planar-mirror resonators. They enable also the realization of highly-efficient corner-cube retro reflectors.

In this work, we present laser-quality low-loss Bragg mirrors exhibiting a broad omnidirectional stop band in the mid-infrared around 1500 cm^{-1} with a nominal reflectivity higher than 98 % over a wide range of 650 cm^{-1}. This is possible due to the high refractive index contrast between the mirror materials as well as between the low-index material and the ambient medium. For detailed optical analysis of the angle dependent reflectivity of the mirrors, a high-finesse microcavity formed by two such Bragg mirrors was used. The appearance of a cavity resonance facilitates the accurate determination of the mirror reflectivity by evaluating the quality factor of the resonator. The high reflectivity of the Bragg mirrors is confirmed by the fact that similar mirrors have successfully been used for cw operating mid-infrared vertical-cavity surface-emitting lasers with low thresholds.

The molecular-beam epitaxially grown microcavity sample is designed for a wavelength of 7 µm and consists of a four-period bottom and a three-period top PbTe/EuTe Bragg mirror with a λ/2 PbTe cavity region in between. High-resolution Fourier transform infrared (FTIR) transmittance measurements were used for the full characterization of the omnidirectional mirrors. The special choice of the mirror materials ensures open optical gaps for TM as well as for TE polarization with air as ambient medium. The sufficiently high refractive index contrast between the materials avoids also to satisfy the Brewster angle condition for any interface in the multilayer stack. The stop band width observed for angles of incidence up to 80° was determined at 3 % transmittance at the high and low energy boundaries of the stop band. From this, the relative stop band width of 43 % can be deduced in good agreement to theoretical estimates using the refractive indices of the mirror materials. From the spectral position and the width of the cavity resonance, the angular dependence of the mirror reflectance can be determined.

The experimental results are compared to transfer matrix simulations including a model dielectric function of the materials giving a good agreement between experimental and theoretical results. In addition, the complete optical band structure of the Bragg mirror as one-dimensional photonic band gap structure was calculated, clearly showing the broad omnidirectional reflectance range.

Our result evidences that the material choice of EuTe and PbTe produces highly efficient omnidirectional Bragg mirrors for the mid-infrared range, which are suitable not only for various laser mirror applications but also for cavity ring-down spectroscopy for ultra-high-sensitivity absorption measurements.

UV-Nanoimprinting – A Potential Method for the Fabrication of 3D-Photonic Crystals

T. Glinsner, F. Isfahani, and K. Hingerl
Institute of Semiconductor and Solid State Physics
Johannes Kepler University, A-4040 Linz, Austria

This contribution presents results achieved in ultraviolet nanoimprint lithography (UV-NIL) recommending this process as a potential fabrication method for photonic crystals.

In photonic crystals the periodic arrangement of two materials with dissimilar dielectric properties exhibits a band of forbidden frequencies for the propagation of light (photonic band gap). Several techniques for the fabrication of 3D photonic crystals were proposed. Among them can be found wafer bonding, silicon micromachining, self-assembly, two-photon absorption, 3D holography as well as subsequent sputtering, DUV lithography and etching of consecutive planes.

UV-NIL offers a low cost opportunity for the fabrication of nm-scale pattern transfer in single or multiple step application if compared to mainstream optical lithography. In UV-NIL processes, soft (PDMS) or hard stamps (quartz glass) are used to imprint features into a UV-curable low viscosity material at room temperature. The Industrial Technology Roadmap for Semiconductors (ITRS) calls for nanoimprint lithography to be employed for the 32 nm node, which may be reached in 2010. This next generation lithography technique is using quartz glass stamps, fabricated by e-beam lithography and subsequent dry etching techniques, which can be repeatedly imprinted in spin-on material layers on silicon substrates.

A concept for the fabrication of the woodpile structure will be demonstrated as well as achieved results. The woodpile structure consists of aligned rods where every subsequent layer is rotated 90° above the former layer so that the fifth layer is exactly above the first one and the piles of the third shall be located exactly between the piles of the first row.

Polarization Splitting Based on Planar Photonic Crystals

V. Rinnerbauer [1,2], J. Schermer [2], and K. Hingerl [1]
[1] Christian Doppler Labor für oberflächenoptische Methoden, Johannes Kepler University, A-4040 Linz, Austria
[2] Photeon Technologies, A-6900 Bregenz, Austria

Planar polarization splitting devices based on photonic crystal slabs have been developed, their main advantages being the planar design and their possible integration into PLCs.

Due to their inherent polarization sensitivity, photonic crystals offer convenient solutions on a length scale of several tens of micrometers in silicon-based or other high index material systems. In a 2D photonic crystal slab, the presence of a horizontal symmetry plane allows us to decompose the guided modes into TE-like and TM-like polarization states, which are even and odd with respect to reflections through this plane.

We have developed three different principles for planar polarization splitting devices that exploit the polarization dependency of these guided modes.

The first principle is based on reflection and transmission at a photonic crystal interface. In this case, the photonic crystal acts like a filter that is not only wavelength selective, but also polarization selective. The reflection and transmission spectra of such a photonic crystal layout have been calculated using a plane wave expansion technique, which yields a reflection coefficient of 0.99 for TE and a transmission coefficient of 0.998 for TM for a certain wavelength. The result has also been verified with 2D and 3D FTDT calculations.

The second principle uses a defect waveguide for one polarization, and free propagation through the photonic crystal for the other polarization. In this case TM polarization is allowed to propagate freely through the crystal, whereas TE is restricted to a defect waveguide, by which it is separated from the first one. For an optimized structure, this principle yields more than 93% output power for both polarizations over a broad wavelength range.

In the third principle, defect waveguides with polarization dependent guided modes are used for both polarizations. In this case, careful design and matching of the defect modes is needed for a good transmission characteristic.

These results obtained from numerical simulations show that polarization splitting is possible with high efficiency in photonic crystal slabs. Prototypes of polarization splitters based on the second principle will be manufactured at the University of Linz.

Electronic and Magnetic Properties of GaN:Fe

A. Bonanni [1], H. Przybylinska [1,2], A. Wolos [1], C. Simbrunner [1], H. Sitter [1], W. Jantsch [1], M. Kiecana [2], M. Sawicki [2], T. Dietl [2], P. Granitzer [3], K. Rumpf [3], and H. Krenn [3]

[1] Institute of Semiconductor and Solid State Physics, Johannes Kepler University, A-4040 Linz, Austria
[2] Institute of Physics, Polish Academy of Sciences, PL-02-668 Warsaw, Poland
[3] Karl Franzens Universität, A-8010 Graz, Austria

Transition metal doped GaN is one of the predicted candidates for obtaining Zener-type ferromagnetism with $T_c > 300$ K. As a necessary condition, the transition metal ion should be incorporated on isolated (*i.e.* not clustered) substitutional sites and exhibit a high-spin ground state. So far, the Mn dopant in GaN has been investigated thoroughly, as it was expected to act as an acceptor providing beside the S=5/2 spin also the high hole concentration necessary to mediate the exchange coupling among the Mn ions. More recently it has been shown, however, that unlike Mn in GaAs the 3+/2+ acceptor level of Mn in GaN is deep (>1.4 eV above the valence band edge) and the hole is localized on Mn, leaving it in the $3d^4$ state. Hence, Zener magnetism is not expected for the GaN:Mn system. In this respect the GaN:Fe seems to be more promising, especially with p-type codoping.

Here we report on MOCVD growth of GaN:Fe and its characterization by means of high-resolution X-ray diffraction (HRXD), secondary ion mass spectroscopy (SIMS), photoluminescence (PL), Hall-effect, electron spin resonance (ESR), and SQUID magnetometry. Both ESR and PL demonstrate the existence of Fe in the isolated $3d^5$ (3+) state. The susceptibility shows, apart from Curie paramagnetism due to Fe^{3+}, a temperature independent contribution which we attribute tentatively to van Vleck paramagnetism of Fe in the 2+ state. The coexistence of Fe in the two charge states is confirmed by the observed metastable increase of the Fe^{3+} ESR signal after illumination with UV light. The fraction of Fe^{3+} ions was also found to increase upon additional co-doping with Mg acceptors, both in ESR as well as in susceptibility. A significant reduction of the temperature independent magnetic moment was simultaneously observed. High field SQUID data yield an Fe concentration in the $x \approx 10^{-3}$ range, comparable with SIMS results.

High Mobility Si/SiGe Heterostructures for Spintronics Applications

D. Gruber, H. Malissa, G. Chen, D. Pachinger, H. Lichtenberger, T. Fromherz, F. Schäffler, G. Bauer, and W. Jantsch
Institute of Semiconductor and Solid State Physics
Johannes Kepler University, A-4040 Linz, Austria

The Silicon-Germanium (SiGe) material system is a promising candidate for solid-state spintronics applications due to its very long relaxation lifetimes [1] and its compatibility to standard Si device processing technology. The required high electron mobilities can be reached by using thick graded $Si_{1-x}Ge_x$ buffers with $0.2 < x < 0.3$ and low temperature modulation-doping with Sb of the strained Si/SiGe quantum well(s). In this work we report about the molecular beam epitaxy (MBE) growth and processing of 2d samples that reach μ of up to 250000 cm^2/Vs at low temperatures and of quantum dots grown on prepatterned substrates. We report on the spin properties evaluated from conduction electron spin resonance, CESR.

The high quality of our layers is also evidenced in recent magneto-transport experiments [2]: They show well pronounced quantum Hall effect (FQHE) features, where the ν=1/3, 3/5 and 4/9 states are seen for the first time ever in the SiGe material system.

The spin properties of conduction electrons in 2d quantum wells and in Si quantum dots were investigated by CESR. On two-dimensional channels we find anisotropy of the line width, the longitudinal spin relaxation and the g-factor. These anisotropies increase with increasing carrier density which can be explained consistently in terms of the Bychkov-Rashba field which arises from the built-in electric field at the quantum well. Using two coupled quantum wells – a pure Si well and another one with up to 10% Ge admixture - and front- and back-gate electrodes, we show that the g-factor of the conduction electrons can be adjusted by an externally applied electric field which may be used for spin manipulation [3].

Lateral confinement is achieved by MBE growth of Ge dots, either (i) in the self-organized Stranski-Kastranow mode, or by making use of seeded growth (ii) on prepatterned substrates prepared by e-beam or holographic lithography. In both cases, the resulting Ge dots were overgrown by a few monolayers of Si, which are strained. Consequently, locally an attractive potential results for conduction electrons in the Si layers. This effect is reinforced by alternating growth of Si layers and stacked, vertically ordered Ge dots (up to 24 periods) on an area of up to 3x6 mm^2 yielding more than 10^{10} quantum dots.

Such structures show the well known fairly wide photoluminescence (PL) band centred at 0.8 eV which is due to spatially indirect transitions from the valence band of the Ge dots to the confined Si conduction band states. In ESR a single line is seen with a g-factor close to 2.0000 during illumination with sub-bandgap light. In a series of differently prepared samples, this signal correlates in amplitude with that of the PL-band. The linewidth of the ESR signal of 0.3 G is smaller than that of typical donors by a factor of 10 but an order of magnitude higher than that of the 2d electrons. We attribute this broadening to inhomogeneous size distribution and the hyperfine interaction of electrons in the dots with ^{29}Si and ^{73}Ge.

[1] A.M. Tyryshkin, S.A. Lyon, W. Jantsch, F. Schäffler, cond-mat/0304284 and PRL, in print.

[2] K. Lai, W. Pan, D.C. Tsui, S. Lyon, M. Mühlberger, F.Schäffler, PRL. 93, 156805 (2004)

[3] H. Malissa, W. Jantsch, M. Mühlberger, F. Schäffler, Z. Wilamowski, M. Draxler, P.Bauer, Appl. Phys. Lett. **85**, 1739 (2004)

Quantitative Scanning Capacitance Spectroscopy on GaAs and InAs Quantum Dots

W. Brezna, T. Roch, G. Strasser, and J. Smoliner
Institute of Solid State Electronics
Vienna University of Technology, A-1040 Vienna, Austria

Scanning Capacitance Microscopy/Spectroscopy (SCM/SCS) is an extension of conventional Atomic Force Microscopy (AFM) and a promising tool for two-dimensional carrier profiling in semiconductor devices. In SCM/SCS, a conductive AFM tip is used to measure the local capacitance between the tip and the sample. The current state of the art of this technique can be found in the review articles [1] – [3].

In scanning capacitance spectroscopy (SCS), the tip-sample capacitance is recorded during a DC voltage sweep to obtain a capacitance versus voltage (C(V)) curve [4]. However, quantitative SCM/SCS measurements are still a major challenge for technical and physical reasons. To circumvent at least the reproducibility problems with reference samples, quantitative scanning capacitance spectroscopy can be used. In previous work done by our group [5] we have demonstrated that this method is e.g. useful for a nanoscale analysis of high-k dielectric materials such as ZrO_2 and a point-wise calibration of capacitance images obtained by commercial SCM systems.

While a large amount of literature exists on SCM measurements on Silicon samples, significantly fewer publications can be found on SCM on GaAs and other III-V materials. Besides very innovative approaches such as X-ray absorption measurements by SCM [6] and local capacitance measurements on InAs dot-covered GaAs surfaces by scanning capacitance microscopy [7] under high vacuum conditions, most of the SCM work on GaAs was devoted to the SCM characterization of laser structures [8]. Douheret, e.g., has shown that SCM can provide a complete 2D map of the device structure, including doping variations, the location of p-n junctions and regrown interfaces.

The current activity of our group is to investigate bulk GaAs and InAs quantum dots by quantitative scanning capacitance spectroscopy in ambient atmosphere. It is found that the experimental data agree well with capacitance spectra calculated from a simple spherical capacitor model. The donor concentrations obtained from this model are in excellent agreement with the sample parameters and the measured Schottky barrier heights are consistent with data obtained by Ballistic Electron Emission Microscopy on similar samples [9]. The influence of illumination and tip force is found to be very critical.

We also found a force threshold for reproducible capacitance measurements and a significant influence of the tip sample force on the obtained results.

[1] V.V. Zavyalov, J.S. McMurray, C.C. Williams, Rev. Sci. Instr. 7, 158 (1999)
[2] R.Stephenson, P.DeWolf, T.Trenkler, T.Hantschel, T.Clarysse, P.Jansen, W.Wandervorst, Vac. Sci. Technol. B18, 555 (2000)
[3] D.D.Bugg, P.J.King, J. Phys. E21 147 (1988)
[4] E.H. Nicollian, J.R. Brews, MOS (metal oxide semiconductor) physics and technology, John Wiley & Sons Ltd, New York 1982
[5] W.Brezna, M.Schramboeck, A.Lugstein, S.Harasek, H.Enichlmair, E.Bertagnolli, E.Gornik, J. Smoliner, Appl. Phys. Lett. 83 4253 (2003)
[6] M.Ishii, T.Uchihashi, Physica B 340-342, 1142 (2003)
[7] H.Yamamoto, T.Takahashi, I.Kamiya, Appl. Phys. Lett. 77, 1994 (2000)
[8] O.Douheret, S.Anand, C.Angulo-Barrios, S.Lourdudoss, Appl. Phys. Lett. 81, 960 (2002)
[9] D.Rakoczy, G.Strasser, J.Smoliner, J. Vac. Sci. Technol. B20, 373 (2002)

Self-Organisation of Ripples and Islands with SiGe-MBE

G. Chen, H. Lichtenberger, G. Bauer, and F. Schäffler
Institute of Semiconductor and Solid State Physics
Johannes Kepler University, A-4040 Linz, Austria

The self-organized growth of the Ge/Si quantum dot heterostructure system has attracted considerable interest, aiming at its potential for electronic and optoelectronics devices, due its compatibility with the well-explored Si technology. Recently, laterally ordered quantum Ge/Si dots have also been suggested for the implementation of quantum computing functions, as well as quantum information storage, which both require the separate identification and external addressability of each quantum dot.

A straightforward approach is to deposit Ge/SiGe onto pre-patterned Si substrates, which are prepared via lithography and subsequent reactive ion etching (RIE). Almost perfect lateral ordering of Ge island arrays with periodicity down to 250 nm has been achieved on Si(001) substrates prepatterned by e-beam lithography. AFM images show that the nucleation site of SiGe islands depends strongly on the surface morphology of the templates after Si buffer layer growth. If the buffer layer is thick enough it converts the RIE-etched pit arrays into a smoothly varying, facetted landscape, which is dominated by arrays of shallow inverted {11n} pyramid pits with a slope angle of ~5° on a rather flat surface. Upon SiGe wetting layer growth, a transition of the facets from {11n} to low-energy {105} facets would onset through the formation of ripples with {105} facets and (001) surfaces. This results from a well-understood, strain-driven step-meandering instability. The intersections of these facets are defined by ripples along two orthogonal <110> directions. With more SiGe deposition, SiGe islands nucleate first at the deepest point of the pits, and then at the intersection point of the ripples. At high enough SiGe or Ge coverages, the AFM images show dome structures with {105}, {113}, {15,3,23} facets. In contrast, if the depth of the pits exceeds the buffer layer thickness, truncated Si pyramids and steep inverted pyramid pit arrays with {113} and {117} facets form during buffer deposition. In this case, SiGe island nucleation occurs at the saddle points between two neighboring Si pyramids with a rhomboid pyramid structure, and at the top of these truncated Si pyramids as tiny huts.

An alternative way to achieve ordering is to use a slightly vicinal Si(001) surface, which is intrinsically unstable against kinetic step-bunching during homoepitaxial growth. The height and period of the step bunches depend on miscut angle, growth temperature, growth rate and epilayer thickness. By increasing the substrate miscut to 4° we reduced the period of the evolving step-bunching structure to create a Si template with pronounced ripples showing a spacing of 100±10 nm, and a corrugation height of ≈5 nm. A $Si_{0.55}Ge_{0.45}$ layer deposited at intermediate 550 °C relieves stress by forming {105}-faceted islands, which would form the well-known hut-clusters on flat (001) surfaces. Due to the substrate miscut, however, the islands are bound by only two {105} facets on the downhill side of the bunches, and the (001)-facet on top. Further away from thermal equilibrium, the $Si_{0.55}Ge_{0.45}$ film deposited at 425 °C does not completely disintegrate into individual islands, but reveals how and where island nucleation commences: Upon SiGe deposition the flanks of the step bunches are converted into a zigzag train of adjacent $(\bar{1}05)$ and $(0\bar{1}5)$ facets. The originally smooth flanks with typically ~8° inclination with respect to [001] are energetically favorable nucleation sites for the strained SiGe epilayer, leading to a {105}-faceted ridge structure, which is perpendicular to the step-bunches. This is a step-meandering instability induced by the low-energy {105} facets of SiGe on Si(001), which marks the transition from conformal Si/SiGe epilayer growth to strain-driven, ordered 3D-growth which is observed at 625°C for the $Si_{0.55}Ge_{0.45}$ epi-layer.

Photocurrent Spectroscopy of Single InAs/GaAs Quantum Dots

G. Fasching [1], F. Schrey [1], K. Unterrainer [1], W. Brezna [2], J. Smoliner [2], T. Roch [2], M. Andrews [2], and G. Strasser [2]
[1] Institute of Photonics and Centre for Micro- and Nanostructures
[2] Institute of Solid-State Electronics and Centre for Micro- and Nanostructures
Vienna University of Technology, A-1040 Vienna, Austria

Quantum dots provide a strong three dimensional carrier confinement resulting in atomic like, discrete energy levels. The δ-function-like density of states predestine dots to be used either as ensemble in lasers [1], MIR photodetectors [2] or in single QD devices, such as single-photon turnstile devices [3], and single-electron turnstile devices [4].

In this contribution, we report on photoluminescence and photocurrent measurements of InAs quantum dots embedded in a quantum dot photodiode. QDs provided with both electric contacts and optical access allow us to vary independently the electric field while measuring the optical or electrical response of the dots. The photoluminescence is recorded with a micro luminescence setup in combination with a nitrogen cooled CCD. At 4 K and an excitation power of 40 W/cm^2 the single dot PL exhibit ground state transitions at 1278 meV and a linewidth of 53 μeV. For the PC measurements we use a tunable cw Ti:Sapphire laser to resonantly excite the quantum dot energy levels, and a self-built high sensitive current-voltage converter for the detection of the photocurrent. As a function of the applied voltage a linear Stark shift of 4.3 meV/V is observed. The strong Stark shift can be used for the realization of a single quantum-dot-spectrometer, which is tunable by the QCSE, and the photons are detected by simply measuring the PC of a single quantum dot. We have shown in previous work [2] that the PL and PC transition energies of dot ensembles can be adjusted by embedding them into a two dimensional superlattice. This implies the possibility to control carrier scattering like thermo-ionic emission and therefore the reduction of the dephasing in single-dot tunneling processes.

[1] G. Park et al., IEEE Photon. Tech. Lett. **12**, 230 (2000)

[2] L. Rebole et al., Appl. Phys. Lett. **81**, 2079 (2002)

[3] P. Michler et al., Science **90**, 2282 (2000)

[4] A. Zrenner et al., Nature **418**, 612 (2002)

Lateral Quantum Dots in High Mobility Heterostructures

G. Pillwein [1], T. Berer [1], G. Brunthaler [1], F. Schäffler [1], and G. Strasser [2]
[1] Institute of Semiconductor and Solid State Physics,
Johannes Kepler University, A-4040 Linz, Austria
[2] Institute of Solid State Electronics
Vienna University of Technology, A-1040 Vienna, Austria

In several recent proposals [1] – [3] lateral quantum dots were discussed as a promising option to realize the quantum entanglement necessary for quantum computation. We have fabricated single lateral quantum dots in the two-dimensional electron gas (2DEG) of modulation doped GaAs/AlGaAs and Si/SiGe heterostructures, which are basic elements for more sophisticated devices.

One type of investigated quantum dots is based on MBE grown GaAs/$Al_{0.3}Ga_{0.7}As$ heterostructures with a 2DEG situated 70 nm below the sample surface. They have a carrier concentration of about 2×10^{11} cm^{-2} and a mobility of up to 1.4×10^{6} cm^2/Vs. Ohmic contacts were made from an Au/Ni/Ge alloy, and Hall bar mesas were wet-etched. The quantum dot structure was defined by e-beam lithography and subsequent deposition of Cr/Au metal electrodes (i.e. the split gates) on top of the Hall bar mesa. The design consists of four gate fingers to define a quantum dot. The two outer gates and the bottom gate define the tunnel barriers, which separate the quantum dot area from the surrounding 2DEG. The center (plunger) gate can be used to change the electrostatic potential of the dot.

Electrical measurements were carried out in a ^3He cryostat at a temperature of 300 mK and in a $^3He/^4He$ dilution refrigerator at 30 mK using a low frequency lock-in technique. By applying negative voltages to the split gates, a quantum dot is formed in the underlying 2DEG. We measured the differential conductance dependent on both V_G and V_{SD}, resulting in Coulomb diamonds. From these the basic properties of the quantum dot are obtained, including total and source capacitance as well as an estimate of the actual size of the quantum dot. The active diameter of the smallest dots was about 120 nm, which corresponds to approximately 20 electrons.

The technology of the GaAs structures has been adapted to Si/SiGe-based lateral quantum dots. Recently, several lateral quantum dots in silicon/silicon-germanium heterostructures have been reported [4], [5]. However, none of these were achieved by the classical split-gate technique that is necessary for the coupling of quantum dots and for high integration. We report Coulomb blockade measurements of a lateral quantum dot formed by the split-gate technique on a MBE grown modulation doped Si/$Si_{0.75}Ge_{0.25}$ heterostructure.

Electrical measurements at 1.5 K showed an electron mobility of 150000 cm^2/Vs at an electron density of 3.2 x 10^{11} cm^{-2}. Ohmic contacts were formed by deposition of Au/Sb and subsequent annealing at 350 ºC. A Hall-bar structure was prepared by reactive ion etching (RIE) with SF_6. The split gate structures were written by e-beam lithography and defined by lift-off of the Schottky-gate metal Pd.

By analyzing the measured Coulomb diamond we estimated the dot diameter to be 100 nm resulting in 26 electrons in the dot.

[1] D. Loss and D. P. Vincenzo, Phys. Rev. A, **57**, 120 (1998)
[2] L.M.K. Vandersypen et al, quant-ph/0207059 (2002)
[3] M. Friesen *et al.*, Phys. Rev. B, **67**, 1213010-1 (2004)
[4] A. Notargiacomo *et al.*, APL **83**, 302 (2004).
[5] L. J. Klein *et al.*, APL **84**, 4047 (2004).

Self Organized InAs Quantum Dot Arrays on Patterned GaAs Substrates

M. Schramböck, W. Schrenk, T. Roch, A. M. Andrews, M. Austerer, and G. Strasser
Center for Micro- and Nanostructures
Vienna University of Technology, A-1040 Vienna, Austria

Self-assembled semiconductor nanostructures such as quantum dots (QDs) have been under intense investigation during the last years due to their appealing electronic and optical properties. Unique physical properties have been observed in QD structures, and device applications using QDs, such as lasers, detectors and memories, have been explored. However, for novel QD devices like single photon sources or transistor structures, it is desirable to control the lateral position of the QDs. To achieve this, nanoscale grid patterns can be used to laterally align the QDs.

In this work, the self organization of InAs quantum dots grown with molecular beam epitaxy (MBE) on pre-patterned GaAs substrates was investigated. To create the grid patterns on the substrates, holographic lithography has been used.

Holographic lithography was studied because it provides an easy and efficient way to create nanosized patterns over large areas. For holographic lithography a He-Cd laser at a wavelength of 325 nm was used as an ultraviolet (UV) light source. After coating the GaAs substrate with photoresist it was then exposed in a holographic apparatus. The nanoscale grid patterns were then transferred onto the GaAs using wet chemical etching.

After preparing the substrates they were thoroughly cleaned, inserted into the MBE chamber and prepared for the growth. After growing a GaAs-based buffer layer on the substrates, they were consequently covered with self assembled QDs. These dots are either embedded into GaAs or serve as surface dots for further investigations.

The dot density, lateral and size distribution is measured using atomic force microscopy (AFM). Photoluminescence (PL) measurements performed on the samples with and without patterns give further information on dot size and size distribution. Furthermore, the influence of different dot growth conditions on dot quality and density is examined.

Ultrafast Intersublevel Spectroscopy of a Single Quantum Dot

F.F. Schrey, G. Fasching, T. Müller, G. Strasser, and K. Unterrainer
Institute for Photonics and Centre of Micro- and Nanostructures
Vienna University of Technology, A-1040 Vienna, Austria

The strong interest in mid- (MIR) and far-infrared spectroscopy demands very efficient emitters and detectors. For the latter case quantum dot (QD) based detectors (QDIPs) show very promising results due to the discrete electronic states [1]. In addition, QD intersublevel transitions are discussed to improve the performance of quantum cascade lasers [2]. However, both applications are limited by intersublevel relaxation properties.

We tune mid-infrared (MIR) probe pulses (40 fs) into resonance with intersublevel transitions of undoped InAs QDs to measure the intersublevel dynamics after excitation by an ultrashort (12 fs) NIR interband pump pulse [3]. The electron capture time decreases with increasing excitation density from 2.7 ps to 1.5 ps, which can be explained by electron-electron scattering. The temperature-dependence of the capture time is well explained by a stepwise relaxation process trough excited QD states under multi-phonon emission. In order to exclude possible ensemble related processes, this pump and probe technique (P&P) has to be extended into the single QD (SQD) region. So far direct detection of MIR signals in the InAs SQD case is impossible. Hence we exploit the idea that the sublevel population can be determined by NIR exciton luminescence. In a micro-photoluminescence (μPL) experiment with superimposed MIR excitation we prove that the NIR luminescence can be used to probe the influence of the MIR excitation [4]. We observe a direct MIR induced electron transfer between excited QD states. Combining the μPL and P&P experiments we can investigate the electron dynamics within a SQD after the pump pulse excited electrons have relaxed from the WL into the dots by applying MIR probe pulses. The NIR interband recombination luminescence is recorded as function of the time delay between the NIR and MIR pulses. We present first results for the dynamics of the MIR mediated electron level coupling in an InAs SQD.

[1] L. Rebohle et al., Appl. Phys. Lett. 81, 2079 (2002)

[2] S. Anders et al., Appl. Phys. Lett. 82, 3862 (2003).

[3] T. Müller et al., Appl. Phys. Lett. 83, 3572 (2003)

[4] F.F.Schrey et al., phys. stat. sol.(c)1, 434 (2004)

X-Ray Diffraction from a SiGe Island Quasicrystal

J. Stangl, J. Novak, E. Wintersberger, V. Holy, and G. Bauer
Institute of Semiconductor and Solid State Physics
Johannes Kepler University, A-4040 Linz, Austria

The introduction of small islands with sub-µm size, so-called quantum dots, has increased the design flexibility for semiconductor devices. In order to keep the defect densities low, self-assembled growth of such structures in the Stranski-Krastanov growth mode has proven to be particularly successful. Still, the control of quantum dots produced by self-assembly is demanding in two aspects: (i) The size homogeneity of such quantum dots is usually much worse than in lithographically defined structures. (ii) There is little control over the position of self-assembled nanostructures.

These shortcomings can be diminished if multilayers are grown instead of single layers: due to the strain fields induced by buried dots, dots in subsequent layers nucleate preferentially on top of buried ones (this is true in the SiGe system), leading to regular island arrays. However, these arrays are still not perfectly regular, and also the size homogeneity of islands is not optimized. The latter is important, as the size is coupled to other island properties such as Ge content and relaxation, which influences the optoelectronic properties of the islands.

A promising route towards very regular islands is the growth on prepatterned substrates. In the presented case, a regular quadratic array of pits has been produced by electron lithography. The period of this array is 400 nm in the ⟨110⟩ directions. To ensure defect-free island growth, 150 nm of Si have been deposited on the patterned substrate, followed by 6 ML of Ge at a growth temperature of 700 °C. These islands have been capped with 30 nm of Si, and the island-cap stack was repeated 12 times, with the growth temperature lowered to 650 °C. This resulted in a 3D array of SiGe islands embedded into Si, i.e., the islands form a “quasi-crystal” in the Si matrix.

X-ray diffraction reveals the structure of this quasi-crystal, which manifests itself by a sequence of satellite maxima along growth direction and perpendicular to it in reciprocal space maps (see Fig. 1). The envelope of these satellites contains information about the shape, the strain state, and the Ge content of the buried islands.

To determine these parameters, the reciprocal space map has been fitted using an island model of a truncated cone, performing analytic calculations of the strain fields, and numerical simulations of the scattered intensity. As a result, we obtain a Ge content of about 40% in the buried islands, and we find that the sidewall slope corresponds well to {105} facetted, truncated pyramids. The island dimensions are found to be 170 nm base width and 20 nm width of the top facet. The strain values in the island center reach 0.9% laterally and 3.4% vertically (measured with respect to the Si substrate).

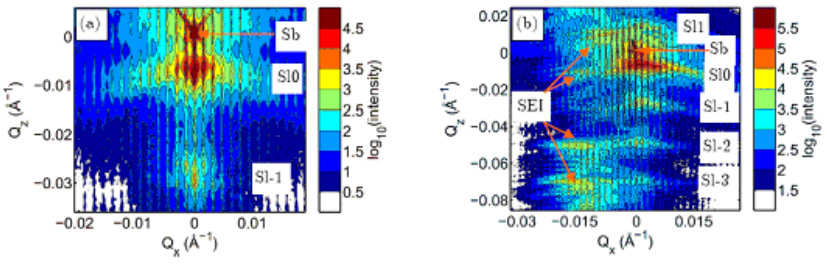

Fig. 1: Measured reciprocal space maps around the (224) (a) and (004) (b) Bragg reflections.

Cross Sectional Ballistic Electron Emission Microscopy for Schottky Barrier Height Profiling on Heterostructures

D. Rakoczy, G. Strasser, and J. Smoliner
Institute of Solid State Electronics
Vienna University of Technology, A-1040 Vienna, Austria

BEEM is a three terminal extension of Scanning Tunneling Microscopy (STM), where the STM tip is used to inject hot electrons into a semiconductor via a thin metallic base layer. If the electron energy is high enough to overcome the Schottky barrier height at the metal-semiconductor interface, the electrons can penetrate into the semiconductor. The corresponding current, measured vs. the tunneling bias using a backside collector contact, is called BEEM spectrum. By mapping the BEEM current for a constant tip bias while scanning the sample surface, also images can be taken with a spatial resolution of about 10 Å.

As cross sectional STM techniques are widely utilized to study problems in surface physics and are especially useful for the characterization of MBE grown GaAs-AlGaAs heterostructures, it seems to be a straightforward idea to combine cross sectional STM and conventional BEEM, resulting in cross sectional BEEM (XBEEM). However, no XBEEM experiments are reported in the literature to our knowledge until now. In our opinion, this is primarily due to technical problems. Using an appropriate experimental setup, XBEEM turns out to be a very useful technique, for instance, to determine band offsets of GaAs-AlGaAs heterostructures.

The aim of this project was to establish XBEEM as a technique for the investigation of Schottky barrier height profiles on MBE grown heterostructures in cross-sectional geometry. The sample design used for the first XBEEM measurements was a GaAs-AlGaAs heterostructure with the following MBE grown layer sequence: On a semi insulating substrate (GaAs [100]), a 3 µm thick layer of n-type GaAs ($N_D = 8x10^{16}$ cm^{-3}) was grown. On top of this layer we grew 5 periods of an AlGaAs-GaAs heterostructure (d_{AlGaAs} = 20 nm, d_{GaAs} = 50 nm) followed by a 200 nm thick GaAs spacer. This layer sequence was repeated three times, however, with layer thicknesses of (d_{AlGaAs} = 50 nm, d_{GaAs} = 20 nm) and (d_{AlGaAs} = 50 nm, d_{GaAs} = 50 nm), respectively. All GaAs layers were doped at a level of $N_D = 8x10^{16}$ cm^{-3}, the AlGaAs layers were doped a level of $N_D = 5.6x10^{16}$ cm^{-3}. The Aluminum content was 30% for all AlGaAs layers. To facilitate cross-sectional BEEM measurements the samples were cleaved and a 7 nm thick gold film was evaporated onto the cleave edge as a base layer. The backside contact was established via InSn pellets which were alloyed into the sample at 430 °C.

While cross-sectional STM images of this sample show only a barely discernible height difference between the GaAs and the AlGaAs layers, the XBEEM images depict the AlGaAs layers as dark lines with a strong contrast to the surrounding GaAs, clearly revealing the different transmission behavior for those two materials.

To generate a Schottky barrier height profile across the heterostructure, a number of BEEM spectra were recorded along the growth axis. The lateral distance between the single data points was 7.2 nm. From the onset of these spectra, the local barrier heights were extracted and used to generate a barrier height profile. This measured barrier height profile turned out to be significantly smeared out compared to the conduction band profile expected from the MBE growth parameters. We attribute this behavior to lateral surface state induced band bending effects along the heterojunction. In addition, we also found some evidence that the barrier height profile is influenced by single impurities in the AlGaAs layers.

High Electron Mobility Organic Field-Effect Transistors using Fullerene Thin Films

Th.B. Singh [1], N. Marjanović [1], G. J. Matt [1], S. Günes [1], N. S. Sariciftci [1], A. Montaigne Ramil [2], A. Andreev [2], H. Sitter [2], R. Schwödiauer [3], and S. Bauer [3]

[1] Linz Institute for Organic Solar Cells (LIOS), Institute of Physical Chemistry, Johannes Kepler University, A-4040 Linz, Austria

[2] Institute of Semiconductor and Solid State Physics, Johannes Kepler University, A-4040 Linz, Austria

[3] Institute of Soft Matter Physics, Johannes Kepler University, A-4040 Linz, Austria

Hot wall epitaxy (HWE) working close to thermodynamical equilibrium is well known as appropriate technique for growing highly ordered organic thin films, including C_{60} films. HWE grown fullerene bases n-channel organic field-effect transistors (OFET) exhibit an electron mobility up to 2.5 cm^2/Vs with on/off ratio >10^5. A solution processed methanofullerene [6,6]-phenyl C_{61}-butyric acid methyl ester (PCBM) OFET also shows a mobility up to 0.2 cm^2/Vs. Optimization of device performance by the use of novel polymeric dielectrics, channel length and film growth conditions will be presented.

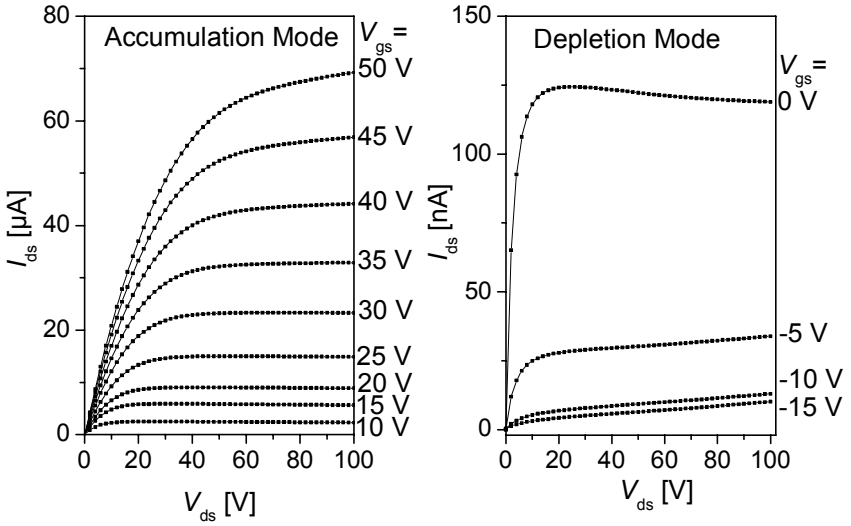

Fig. 1: Transistor characteristics of a C_{60} OFET.

Thermal Imaging at Multiple Time Instants for Study of Self-Heating and ESD Phenomena

V. Dubec [1], S. Bychikhin [1], M. Blaho [1], M. Heer [1], D. Pogany [1], E. Gornik [1], M. Denison, M. Stecher [2], and G. Groos [3]
[1] Institute of Solid State Electronics
Vienna University of Technology, A-1040 Vienna, Austria
[2] Infineon Technologies
D-81617 Münich, Germany
[3] G. Groos
University of Federal Armed Forces
D-85577 Neubiberg, Germany

Protection against electrostatic discharge (ESD) is an important requirement in automotive electronics. For optimization of ESD protection devices (PDs) and for verification of device simulation models it is important to have experimental access to the internal device behavior. Recently a 2D backside transient interferometric mapping (TIM) technique based on fringe interferometry has been introduced for ns thermal energy imaging at single time instant during a single stress event. However, measurements of devices with complex unrepeatable current filament dynamics pattern are time consuming to perform. An extended version of the 2D TIM method suitable for imaging at two time instants during a single stress event has therefore been developed which overcomes the above limitation.

Smart power technology large power DMOS and ESD protection devices developed for automotive applications are investigated. Constant current pulses using a high voltage pulser are used for emulating an ESD pulse.

The backside 2D TIM technique is based on the thermo-optical and plasma-optical effect and uses a Michelson interferometer. For imaging at two time instants, two orthogonally polarized laser beams produced by two high energy pulsed laser sources (λ = 1.3 µm, 5 ns pulses determining the time resolution), combined by a polarizing beam splitter cube are led into the Michelson interferometer. The beams reflected from the device and from the reference mirror are split according to their polarization and create the interference fringe patterns on two infrared (IR) cameras. The laser pulse positions relative to the stress pulse can be chosen independently. The image and waveform acquisition is synchronized and computer controlled. The temperature-related phase distribution in the device at a particular time instant is extracted using a FFT-based method. As two images during a single pulse are possible to record, the method allows the extraction of the instantaneous 2D power dissipation density P_{2D}, which represents the current density distribution in the devices.

The method is applied to the study of moving current filaments in ESD protection devices and DMOSes during a bipolar snapback mode where the current distribution in the device is strongly inhomogeneous. The position and movement direction of the filaments can unambiguously be extracted from few single-shot measurements. The method has a potential for time-efficient studies of destructive phenomena in semiconductor devices including thermal run-away effects in the ns to ms time range.

The project was supported by FP5 IST project DEMAND and Wittgenstein award.

Degradation Mechanisms in AlGaN/GaN HEMTs under Electrostatic Discharge

J. Kuzmík [1], M. Blaho [1], S. Bychikhin [1], D. Pogany [1], P. Javorka [2] and P. Kordoš [2]
[1] Institute of Solid State Electronics
Vienna University of Technology, A-1040 Vienna, Austria
[2] Institute of Thin Films and Interfaces, Research Centre Jülich,
Jülich D-52425, Germany

We study degradation mechanisms in 50 μm gate width / 0.45 μm length AlGaN/GaN HEMTs after electrical overstresses (EOS). Devices may face EOS event during manufacturing, handling, or device operation. Typical current pulses are in the ampere range with duration between nanoseconds and microseconds. The importance of failure mechanism study in III-nitride transistors is given by their potential usage as power devices in many defense and commercial applications where harsh environment conditions can be expected.

100 ns long rectangular current pulses (TLP pulses) are applied on the drain contact keeping either both the source and gate grounded (*gg*) or the source grounded and gate floating (*fg*). Devices were dc characterized after consecutive current stresses. Gate-source *I-V* characteristics were measured to evaluate *Schottky* contact degradation, while *ohmic* contact (R_S, R_D) and open channel resistances (R_0) were extrapolated from the functional dependence of the source-drain resistance on gate voltage. We used backside transient interferometric mapping (TIM) technique to localize current path (dissipated power) in HEMTs during TLP stresses.

In the case of the *gg* stress, holes from the avalanche region are collected also by the gate. Consequently, the premature degradation of the *gg*-stressed HEMT Schottky contact at I_{stress} = 0.45 A can be attributed to the power dissipated directly in the gate contact region. Parameters of the *fg*-stressed HEMT could be analyzed up to I_{stress} = 1.75 A when the gate was damaged. A slight decrease in $R_S + R_D$ is observed initially. Here we assume that at low stress the generated heat was beneficial for additional contact alloying reducing *ohmic* contact resistance if the former annealing was not sufficient. The ohmic contacts catastrophic degradation (ten-fold increase from the nominal value) was recorded at I_{stress} = 1.65 A.

The TIM phase shift characteristics show a fair local maximum at the right edge of the HEMT. Following the change of the stress polarity (drain grounded, source stressed), two new maxima appeared in new positions close to the previous one. These observation correlates with the backside infrared images of the device where dark spot positions correspond to the phase shift maxima on the grounded (opposite) contact. The appearance of dark spots always on the grounded contact suggests that not only the temperature but also current flow direction is decisive for a physical damage formation. We assume that a high electron flow density perpendicularly to the surface is responsible for an electromigration effect and consecutive dark spot formation.

In conclusion, the current filament formation and the electromigration effect were shown to be responsible for the ohmic contact dark spot formation. Dark spots may be considered as a precursor of the ohmic contact degradation. Semiconductor material parameters are not changed substantially during the EOS event.

Direct-Write Deposition Utilizing a Focused Electron Beam

M. Fischer, J. Gottsbachner, S. Müller, and H.D. Wanzenboeck
Institute of Solid State Electronics
Vienna University of Technology, A-1040 Vienna, Austria

The locally confined direct-write deposition is a new, maskless nanostructuring technique that is capable of fabricating 3-D structures within a single process step. The conventional fabrication of nanostructured devices with cutting-edge optical lithography requires the use of cost-intensive phase-shift masks and the processing time for several process steps including blanket deposition of the material, lithographic structuring and etch-back to obtain the desired structures. For prototyping a novel approach using direct-write deposition has been acknowledged as a promising alternative. The energy of a focused particle beam is used to locally induce a chemical vapor deposition. No mask is required and the structures can be deposited within a single process step. A frequently used approach is the deposition of a focused ion beam (FIB). However, the ion contamination originating from the ion source and the atomic mixing of deposited material put a serious constraint on this method. The local deposition can also be induced by a focused electron beam delivering materials with a higher purity and a clear interface to the substrate.

Based on a commercial variable-pressure scanning electron microscope custom-tailored equipment was developed, that allows introducing precursor gases and performing direct-write depositions in the process chamber. A sophisticated gas inlet system with a nozzle system introducing the gas directly to the spot of deposition was designed. The scanning operation of the electron beam could be controlled with a pattern generator, rendering the total specialized setup a unique, versatile nanofabrication tool. For the deposition of material tetraethylorthosilicate (TEOS) was chosen as exemplary precursor, yielding a silicon oxide based material.

The deposition process was investigated and optimized for high deposition rates. The beam current was varied by the aperture setting, and the energy of the electrons could be adjusted via the acceleration voltage in arrange from 1 to 30 kV. The pattern generator allowed varying the pixel spacing of the scan array, the dwell time of the beam on a single spot, and the number of scan repetitions. The variation of parameters was performed by depositing arrays of the material with a univariat parameter change. The surface morphology of the deposited material patches was investigated by atomic force microscopy. A very smooth surface was observed for narrow pixel spacing. The elevated rim on 2 opposing sides of the deposited material results from the longer dwell time of the beam at the left and right edge of the scan pattern.

A correlation of the deposition rate with the acceleration voltage of the beam was made in the range from 30 down to 5 kV. A higher deposition rate was obtained for lower electron energies. At lower primary energy of the beam, the penetration depth of electrons in the material is reduced and the secondary electron yield increases. This result suggests a deposition mechanism based on the interaction with secondary electrons. Also effects of the dwell time and of the pixel spacing were observed. Also the precursor gas pressure was varied, yielding a different surface coverage with precursor molecules required for the deposition reaction. A saturation level could be observed where additional gas could not lead to a further increase of the deposition rate. Concluding, it has been successfully demonstrated that an electron beam may be used as a local probe for the deposition of well defined structures. These findings are considered a solid bias for the better understanding of electron-induced surface reactions and path the way to a further process optimization of this innovative nanofabrication technique.

A New Approach for the Formation of Size and Site Controlled Metallic Nano Dots Seeded by Focused Ion Beams

A. Lugstein, W. Brezna, and E. Bertagnolli
Institute of Solid State Electronics
Vienna University of Technology, A-1040 Vienna, Austria

We present a new approach for the generation of uniform metallic nano dots, which in contrast to conventional bottom up or top down processes is based on a subtractive self organization process relying on material decomposition induced by focused ion beam exposure and subsequent rapid thermal annealing.

The nanometer sized Ga and In dots that can be formed in a size and position controlled fashion were fabricated on GaAs (100), InAs (100), Si (100) and SiO_2 using focused ion beam techniques. Two dimensional ordered arrays of embedded as well as freestanding metallic dots were fabricated by a site control technique relying on preformed craters and an irradiation mediated migration. The diameters of the dots range from 60 to 850 nm.

The formation of these dots is discussed in terms of selective etching of arsenic due to the local energy injection by the ions and further agglomeration. Due to the high energy injection during FIB milling and the low melting point of the metal the precipitations behave like a liquid under milling conditions. Thus, the minimization of surface energy at the enhanced temperatures during FIB exposure calls for a spherical shape of the small droplets, as we did observe.

The morphological evolution of the sample surface was investigated by in-situ FIB-SEM, and AFM, and the chemical composition of the pattern was analyzed using high resolution AES. We completed these many-facetted experimental studies with optical microscopy and electrical measurements.

This technique is a promising way to obtain quantum dot arrays with small and uniform dot sizes and high packaging densities. Since GaAs quantum dot formation from Ga droplets has been reported, our technique is considered to be a candidate for the fabrication of highly ordered quantum dot array structures. Furthermore, this method is expected to apply to various metals apart from Ga and In.

Inductively Coupled Plasma Reactive Ion Etching of GaN

S. Golka, W. Schrenk, and G. Strasser
Center for Micro- and Nanostructures
Vienna University of Technology, A-1040 Vienna, Austria

As etching of GaN cannot be done by wet chemistry to a satisfactory degree, reactive ion etching (RIE) becomes very important, as it is the only means of obtaining vertical structuring. This in particular applies to structures on the micrometer scale where mask thickness is limited by some lithographic technique.

Advanced optoelectronics for the $\lambda = 1.55$ µm regime rely heavily on availability of smooth, vertical etch processes. Depending on application typical waveguide thickness in the GaN system is in the range of 1.5…2.5 µm. Coupling light from standard optical fibers into these waveguides will demand even further etch depth to fabricate etched deep facets or adiabatic tapers. Since GaN commonly grown on Sapphire or SiC cannot be properly cleaved, dry etched mirrors are the only way to implement fiber access.

Unlike GaAs and InP, which are chemically active at least at temperatures above 200 °C, the InGaAlN alloys are very inert even in strong chlorine based chemistry. This lack of chemical reactivity has been solved with high ion acceleration energies in standard RIE reactors. This decreases the mask to etchant selectivity to almost worse than 1:1. This problem can be overcome by high ion density but low bias recipes like those available in ICP reactors.

In this work we developed a $N_2/SiCl_4$ based ICP RIE recipe that overcomes the above problems. A lithographic process with an intermediate SiN_x mask enhances selectivity more, allows for elevated temperatures as is absolutely mandatory for smooth facets if indium is contained in the epitaxy. The $SiCl_4$ is split in the plasma and provides Silicon compounds that are again not reluctant to react with chlorine; these compounds can serve as passivation layers that stick on sidewalls and act as a chemical underetch inhibitor.

We obtain smooth about 5° overcut GaN profiles that are 6 µm high. The selectivity of SiN_X:GaN is 7:1 with an etch rate of 100 nm/min for the GaN. There is no trenching into Al containing epitaxial layers and there is also no trenching at the foot of sidewalls as would be induced by sputtered ion species in standard RIE processes. Consequently, this recipe is compatible with etching of laser/modulator/SOA structures that need lateral electronic transport.

Analytical 3D Hydrodynamical Analysis of Spurious Compressional Wave Excitation by Microacoustic TSM Liquid Sensors

B. Jakoby [1] and R. Beigelbeck [2]
[1] Institute of Sensor and Actuator Systems
Vienna University of Technology, A-1040 Vienna, Austria
[2] Research Unit for Integrated Sensor Systems
Austrian Academy of Sciences, A-2700 Wiener Neustadt, Austria

A typical TSM-resonator for viscosity sensing applications is made of a thin AT-cut quartz disk, which is plated with metal electrodes on both sides of the disk. When applying an electric alternating voltage to the electrodes, the resonator starts to vibrate in thickness-shear-mode. The adjacent liquid is entrained by the shear movement of the immersed TSM-resonator, which leads to a change of the resonance frequency and the damping compared to the vibrating resonator in air. By detecting this shift, the viscosity-density product of the liquid can be determined. In the ideal case, a pure and uniform shear displacement across the resonator surface leads to excitation of an evanescent shear wave in the adjacent viscous liquid. However, in the real case, spurious compressional waves are also excited because of (a) small out-of-plane displacements due to mode conversion (at clamping points, electrode edges, etc.), (b) the uncompensated angular momentum of the dominant shear vibration of the disk.

The resonator is placed in the *xy*-plane of a Cartesian coordinate system. We decouple the piezoelectric disk and the fluid region by considering only the liquid and replace the resonator by impressing a non-uniform Gaussian-shaped shear displacement at the interface as it has been observed in practical measurements. Then, the linearized Navier-Stokes equation in the liquid is solved by using a spectral method. Using this approach, the complete displacement field in the liquid describing both shear as well as compressional waves and their coupling can be expressed by means of compact Fourier double-integrals. The numerical values of these Fourier integrals are approximated by the FFT-algorithm.

The theoretical results are verified by considering the wave excitation of the TSM resonator, which is immersed into a sample liquid (e.g., water). As expected, a dominantly shear polarized wave is excited, which is highly damped when propagating in the z-direction. Simultaneously, two major beams of scarcely damped compressional waves, represented by normal displacements, are built up with increasing z. These major beams reach their maximum only a few hundred nanometers away from the resonator surface. The orthogonal shear component (in y-direction) is a by-product of the excited compressional wave beams and thus the evolution of its peak amplitude with increasing distance z from the resonator shows the same behavior as the compressional components. Due to their finite lateral extension, the pressure waves cause secondary shear components in x- and y- directions with amplitudes being typically two orders of magnitude smaller than the associated normal components. Close to the TSM-surface, these related secondary amplitudes in x-direction are still overshadowed by the primary Gaussian shear displacement.

Simultaneous Measurement of Two Magnetic Field Components Using a Single U-Shaped MEM Cantilever Device

F. Keplinger [1], R. Beigelbeck [2], F. Kohl [2], and P. Loschmidt [2]
[1] Institute of Sensor and Actuator Systems
Vienna University of Technology, A-1040 Vienna, Austria
[2] Research Unit for Integrated Sensor Systems
Austrian Academy of Sciences, A-2700 Wiener Neustadt, Austria

Micromachined cantilevers exhibit an interesting possibility to measure a variety of physical parameters such as magnetization or viscosity. These devices offer a high quality factor and achieve a high sensitivity when they are excited at a resonant frequency. To measure magnetic fields with cantilever structures, the Lorentz force is utilized on a current carrying lead. Cantilevers vibrating in the fundamental mode are typically used to measure the magnetic flux density in the direction parallel to the arms of the cantilever. The presented approach uses high order oscillation modes to measure the flux density in an additional direction of the coordinate system.

The Lorentz force acting on a current-flowed lead is used to bend a micromachined cantilever. Small deflections compared to the length of the cantilever are directly proportional to the applied force. To reach a high sensitivity, the cantilever is excited by a sinusoidal alternating current at the resonant frequency.

The investigated U-shaped cantilever can oscillate in various flexural vibration modes. Among the first four modes are two symmetrical modes (S1 and S2, where the cantilever arms are moving in parallel) and two antisymmetrical modes (A1 and A2, where the arms move in opposite directions).

Each mode can be excited by suitable Lorentz force distributions on different parts of the lead. The fundamental mode S1 is excited by a homogeneous magnetic field in parallel to the cantilever arms. The current path in the arms of the cantilever is parallel to the magnetic field and therefore the forces are generated only at the base of the “U”. The first antisymmetrical mode A1 is excited by a homogeneous magnetic field parallel to the “U”-base, where the Lorentz forces develop only along the arms of the cantilever. Due to the different orientation of the electrical current, one arm is bending up and the other is bending down.

The oscillating cantilever structure can be described by the classical Euler-Bernoulli beam dynamics theory leading to a set of three (one for each cantilever arm and one for the cantilever base) coupled linear 4th-order partial differential equations.

The vibrations of the cantilever are contact-free sensed using an optical readout. The IR-beam of a commercially available reflective sensor is returned partially by the surface of the gold lead on top of the cantilever and received by the photo transistor of the reflective sensor.

To excite the first symmetric (S1) and the first antisymmetrical mode (A1) simultaneously, the appropriate flux densities have to be present and the composite AC current should match to the resonant frequencies of the flexural vibration modes. The amplified output signal of the reflective sensor is analyzed by two lock-in amplifiers. Their output signals are proportional to the magnetic flux densities to be measured. The phase information is used to determine the direction of the magnetic field.

Oil Condition Monitoring Using a Thermal Conductivity Sensor

J. Kuntner, R. Chabicovsky, and B. Jakoby
Institute of Sensor and Actuator Systems
Vienna University of Technology, A-1040 Vienna, Austria

In recent years, the monitoring of oil-based liquids has gained increasing importance in various branches of the industry. A prominent example is the condition monitoring of lubrication and insulating oils. In both cases the water contamination of oil often cannot be avoided which seriously influences its performance if certain levels are exceeded. In the case of lubrication oil, excessive water content leads to insufficient lubrication and subsequently to abrasive wear and corrosion. In case of insulation oils, increased water content results in a considerable reduction of the breakdown voltage. Thus, the detection of water content in the oil is of major importance.

Comparing the thermal transport properties of mineral oil and water, it turns out that the latter features a five times higher thermal conductivity. This indicates that thermal conductivity is a potential parameter for the detection of water content in mineral oils. In this contribution we discuss the application of a miniaturized thermal conductivity sensor for the monitoring of water contamination and deterioration processes in mineral oil.

The device consists of a glass substrate with a resistive loop made of molybdenum, simultaneously serving as both heater and sensing element. Molybdenum has been used due to its linear resistance characteristics, which is valid over a wide temperature range. By applying a transient electrical current, the resistive loop and the surrounding medium under investigation start heating up. Recording the corresponding temperature response of the thin-film structure enables the determination of the thermal conductivity and diffusivity of the surrounding medium. According to theoretical considerations, for the steady state, the excess temperature of the sensor becomes essentially determined by the thermal conductivity of the surrounding fluid. The experimental results show that both water contamination and deterioration processes in mineral oil lead to an increased thermal conductivity indicating the potential of thermal conductivity sensors in the field of oil condition monitoring.

The applied measuring method allows us to clearly detect water deterioration in mineral oil, with the restriction however of a maximum measuring time that must not be exceeded to avoid the disturbing influence of the liquid boundary. To overcome this problem a transient measurement lasting several hundred milliseconds could be utilized. By means of numerical simulations we found that due to the relatively thick glass substrate, the sensitivity in the initial transient regime is decreased accordingly. Utilizing a thinner substrate would significantly increase the sensitivity of the device but at the same time reduce the mechanical robustness of the sensor. Regarding the applicability of the thermal conductivity sensor, thus, in harsh industrial environments, a trade-off has to be found between sensitivity and mechanical robustness.

Microsensor for the Measurement of the Transepidermal Water Loss of Human Skin

M. Mündlein [1], R. Chabicovsky [1], J. Nicolics [1], B. Valentin [1], P. Svasek [2], E.Svasek [2], T. Komeda [3], H. Funakubo [3], T. Nagashima [3], and M. Itoh [3]
[1] Institute of Sensor and Actuator Systems
Vienna University of Technology, A-1040 Vienna, Austria
[2] Ludwig Boltzmann Institute of Biomedical Microtechnique,
A-1040 Vienna, Austria
[3]Shibaura Institute of Technology
Department of Machinery and Control Systems, Saitama-City, 330-8570 Japan

Recently we have developed a novel microsensor to measure the emission of water from human skin. Measurement of the transepidermal water loss (TEWL, expressed in grams per square meter and per hour) is used for studying the water barrier function of the skin. The more perfect the skin protective coat, the higher the water content and the lower the TEWL. Normal skin allows water loss only in small amounts; in the case of atopic skin (atopic dermatitis) the TEWL is high.

The sensor consists of a ceramic substrate (5 mm x 5 mm x 0.6 mm) carrying an interdigital electrode system covered with a highly hygroscopic salt film. It is mounted inside a closed chamber arrangement in a distance of about 1.4 mm away from the skin. The electrodes consist of a double layer of molybdenum and gold. The molybdenum film has been deposited by rf-sputtering; the rather thick gold film (8 µm) has been produced by electroplating. The width of the electrodes is about 55 µm; the gap between the interdigital electrodes is approximately 15 µm. The active moisture sensing area is 1.75 mm x 3.15 mm. The contacts are made of a sputtered layer system of molybdenum, nickel chrome, and gold. The lead-in wires are guided through funnel-shaped holes (laser-drilled) to the rear substrate surface and are bonded to the contacts by using an isotropically conductive adhesive.

Measurements have been carried out at a constant frequency of 500 kHz and a measuring voltage of 100 mV by using a Precision LCR-Meter HP 4285A. We have measured the change of capacity of the electrode system as a function of the TEWL value (received by a Tewameter TM210, Courage + Khazaka Electronic GmbH, Köln) using an equivalent circuit R parallel C. These measurements have been carried out at the left forearm of male subjects with a measuring interval of 20 s. We demonstrate the different measuring results with normal skin and atopic skin.

Particle Discrimination with an Improved Projection Cytometer

J.H. Nieuwenhuis [1], P. Svasek [2], P.M. Sarro [3], and M.J. Vellekoop [1]
[1] Institute of Sensor and Actuator Systems, Center for Micro and Nanostructures, Vienna University of Technology, A-1040 Vienna, Austria
[2] Ludwig Boltzmann Institute of Biomedical Microtechnology, A-1040 Vienna, Austria
[3] Laboratory of ECTM – DIMES, Delft University of Technology, NL-2600 Delft, The Netherlands

An integrated cytometer is presented based on optical projection. A sheath flow focuses the particles closely over an integrated optical sensor capable of counting, sizing and measuring the shape of particles. Measurements demonstrate good repeatability and the ability to discriminate between particles based on their optical properties.

Cytometers are instruments for particle analysis based on the optical properties of the particle. In literature different integrated sheath-flow chambers have been presented (some early ones can be found in [1], [2]), but the optical sensors are often located off-chip. In this paper an integrated projection cytometer is presented that has a built-in optical sensor.

The device (Fig. 1) consists of a transparent flow-channel that has an elongated photodiode (1 x 50 μm^2) integrated in the bottom of this channel, aligned perpendicular to the direction of flow. By means of a non-coaxial sheath flow the sample liquid containing the particles is focused over the optical sensor. The chip is illuminated from the top and when a particle now passes over the sensor its optical properties are registered. The small projection distance realized by the sheath-flow minimizes the optical distortion of the particle projection, without the need for any additional optical components.

The shape of the sensor signal, caused by a passing particle, depends on the optical properties of the particle (Fig. 2). Since the sensor only consists of a single photodiode the optical properties of the particle are integrated along a line perpendicular to the direction of flow.

[1] R. Miyake, H. Ohki, I. Yamazaki, R. Yabe, A Development of Micro Sheath Flow Chamber, proc. of MEMS '91, 1991, pp. 265-270.

[2] D. Sobek, A.M. Young, M.L. Gray, S.D. Senturia, “A microfabricated flow chamber for optical measurement in fluids”, proc. MEMS '93, 1993, pp. 219-224.

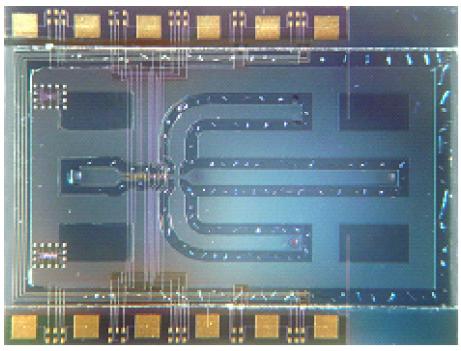

Fig. 1: The cytometer chip (1.5 x 2 cm2)

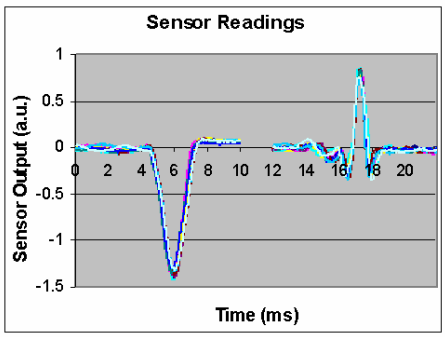

Fig. 2. Measurements for 10 µm radius silver coated particles (left) and 12 µm radius plain particles (right)

SU-8-Based Fluidic Devices

P. Svasek [1], E. Svasek [1], M. Vellekoop [2], and B. Lendl [3]
[1] Ludwig Boltzmann Institute of Biomedical Microtechnology
Vienna University of Technology, A-1040 Vienna, Austria
[2] Institute of Sensor and Actuator Systems
Vienna University of Technology, A-1040 Vienna, Austria
[3] Institute of Chemical Technologies and Analytics
Vienna University of Technology, A-1060 Vienna, Austria

During the last years SU-8 has become a widely used material for MEMS and miniaturized fluidic devices. It can be deposited by spin- or spray coating in a wide range of layer thickness. Because of the low UV absorption of the resist a standard UV mask aligner can be used for exposure, even for thick layers up to a thickness of 1000 µm.

To use FTIR-spectroscopy as a powerful detection method in capillary electrophoresis an *infrared transparent flow cell* had to be designed because the fused silica capillaries normally used in CE are not transparent to IR. An appropriate material for infrared transparent devices is CaF_2 because of its excellent optical properties. The cell consists of two plates of CaF_2, each 1 mm thick. On one of these plates there is a Titanium structure which acts as an optical aperture. The channel is formed by two lines of SU-8 on each CaF_2 plate, each of them 100 µm wide. The distance between these two lines is 150 µm. Their height is 7.5 µm, half of the desired height of the cell. Two wafers (one with metal structure and one without) are superimposed, aligned and pressed against each other during the hardbake process. Consequently the corresponding SU-8 structures are bonded together because the temperature of 200 °C induces complete crosslinking of the SU-8. The final dimension of each cell is 2 x 5 x 2 mm^3. Two capillaries (I.D. 50 µm) are coupled to the cell by means of a metal support and O-ring gaskets.

A micromixer for FTIR-Spectroscopy is used for the investigation of chemical reactions by FTIR-spectroscopy combined with in-situ mixing of two reactants. The IR-beam directly passes the mixing chamber with an optical pathlenght of 10 µm. The mixing device is Y-shaped. Two sheets of liquid are superimposed inside the mixing chamber and mixed by diffusion. Because of the cross-section of the outlet channel (1 mm wide, 10 µm high) the mixing time is approx. 50 ms. The mixer is used in the “stopped-flow-mode”, i.e. the two liquids are injected by means of a double syringe pump. Then the flow is stopped, the reactants are mixed by diffusion and the chemical reaction takes place. This reaction is investigated by time resolved FTIR-spectroscopy. Fabrication of the micromixer is performed by means of a 2-layer lithography, combined with a polymer-based wafer bonding technique. Calcium Fluoride is used as substrate material. A 4 µm thick layer of SU-8 is deposited by spin-coating, softbaked, exposed, post-exposure-baked, but not developed. On top of this layer a 2 µm thick layer of Ag is deposited by evaporation. This metal layer is patterned by wet etching to obtain the structure of the "separation membrane". Finally the SU 8 is developed. Wafer #1 now carries the structures of Inlet 1 and the Separation Membrane. On wafer #2 the structure of Inlet 2 is fabricated as usual from a 4 µm thick layer of SU 8. So far the SU 8 on both wafers is not hardbaked and therefore the polymer is not completely crosslinked. Both wafers are superimposed to form a sandwich, and aligned. Hardbaking is done in an EVG 501 wafer bonder. The wafers are pressed against each other with a force of 1700 N and heated to 200 °C for 1 hour. Because of this high temperature the polymer is completely crosslinked and a bond is established between SU-8 and the Ag structure.